Astronomy & Astrophysics manuscript no. 4107 May 14, 2006
(DOI: will be inserted by hand later)

The role of kink instability in Poynting-flux dominated jets

Dimitrios Giannios and Henk C. Spruit

Max Planck Institute for Astrophysics, Box 1317, D-85741 Garching, Germany

Received / Accepted

Abstract. The role of kink instability in magnetically driven jets is explored through numerical one-dimensional steady relativistic MHD calculations. The instability is shown to have enough time to grow and influence the dynamics of Poynting-flux dominated jets. In the case of AGN jets, the flow becomes kinetic flux dominated at distances $\gtrsim 1000 r_{\rm g}$ because of the rapid dissipation of Poynting flux. When applied to GRB outflows, the model predicts more gradual Poynting dissipation and moderately magnetized flow at distances of $\sim 10^{16}$ cm where the deceleration of the ejecta due to interaction with the external medium is expected. The energy released by the instability can power the compact "blazar zone" emission and the prompt emission of GRB outflows with high radiative efficiencies.

Key words. Magnetohydrodynamics (MHD) – Instabilities – Gamma rays: bursts – Quasars: general

1. Introduction

Relativistic collimated outflows have been extensively observed in active galactic nuclei (AGN) and X-ray binaries (XRB). Gamma-ray bursts (GRB) are also believed to be connected to ultrarelativistic and collimated outflows to overcome the "compactness problem" (e.g. Piran 1999) and to explain the achromatic afterglow breaks (Rhoads 1997; Sari et al. 1999). It is also believed that all these sources are powered by accretion of matter by a compact object.

The widely accepted mechanism for jet acceleration and collimation in the context of AGN and XRB jets is that of magnetic driving. According to this paradigm, magnetic fields anchored to a rotating object can launch an outflow. The rotating object can be a star (Weber & Davis 1967; Mestel 1968), a pulsar (Michel 1969; Goldreich & Julian 1970), an accretion disk (Bisnovatyi-Kogan & Ruzmaikin 1976; Blandford 1976; Lovelace 1976; Blandford & Payne 1982) or a rotating black hole (Blandford & Znajek 1977). The material is accelerated thermally up to the sonic point and centrifugally until the Alfvén point, defined as the point where the flow speed equals the Alfvén speed. After the Alfvén point the inertia of mater does not allow corotation of the magnetic field. As a result, the magnetic field lines bend, developing a strong toroidal component.

Further out the flow passes through the fast magnetosonic point where most of the energy of the flow remains in the form of Poynting flux in the case of relativistic outflows (Michel 1969; Goldreich & Julian 1970; Sakurai 1985; Beskin et al. 1998). Further acceleration of the flow is not straightforward within ideal MHD. It can be shown, for example, that a radial flow is not accelerated after the fast point (e.g. Beskin 1998). This is a result of the fact that the magnetic pressure and tension terms of the Lorentz force almost cancel each other (Begelman & Li 1994). A limited degree of acceleration of the flow is possible if it has a decollimating shape (i.e. the magnetic field diverges faster than radial; Li et al. 1992; Begelman & Li 1994).

Magnetized jets suffer from a number of instabilities. Interaction with the environment causes instabililty of the Kelvin-Helmholtz type and kink instability causes internal rearrangement of the field configuration. Here we focus on kink instability, since it internally dissipates magnetic energy associated with the Poynting flux. As demonstrated elsewhere (Drenkhahn 2002; Drenkhahn & Spruit 2002; Spruit & Drenkhahn 2003) such internal energy dissipation directly leads to acceleration of the flow. Dissipation steepens the radial decrease of magnetic pressure, thereby lifting the cancellation between outward pressure force and inward magnetic tension, and allowing the magnetic pressure gradient to accelerate the flow.

1.1. "AC" versus "DC" outflows

While dissipation of magnetic energy can thus happen through kink instability in an initially axisymmetric ("DC") flow, it can also happen more directly by reconnection in the outflow generated by a non-axisymmetric rotator ("AC" flow). The two cases behave differently in terms of the acceleration profile, and the location and amount of radiation produced by the dissipation process. A non-

Send offprint requests to: giannios@mpa-garching.mpg.de

axisymmetric rotator produces a "striped" outflow (as in the case of a pulsar wind) with reconnectable changes of direction of the field embedded in the flow, and energy release independent of the opening angle of the jet. In the DC case, where energy release is instead mediated by an instability, the rate of energy release is limited by the time it takes an Alfvén wave to travel across the width of the jet. This makes it a sensitive function of the jet opening angle.

The "AC" case has been studied in detail by Drenkhahn (2002), Drenkhahn and Spruit (2002), with application to Gamma-ray bursts. In the case of AGN and XRB, on the other hand, the collimated jet is arguably best understood if the field in the inner disk is of uniform polarity, resulting in an initially axisymmetric flow. Another difference is the lower bulk Lorentz factors in the AGN/XRB case, resulting in faster energy release (in units of the dynamical time of the central engine).

The purpose of this paper is to explore the consequences of magnetic dissipation by internal instability in such axisymmetric (or DC) cases, and its observational signatures. We also apply the calculations to the GRB case, where we compare the results with the AC case studied before.

1.2. Energy release and field decay by the instability

We limit ourselves to a flow with constant opening angle. That is, we leave aside the collimation process. Kink instability is modeled by adding a sink term to the induction equation to account for the non-ideal MHD effects arising from it.

Linear stability theory of kink instability yields a growth time of the order $t_{\rm k} = r\theta/v_{{\rm A},\phi}$ where r is the radius of the jet, θ its opening angle and $v_{{\rm A},\phi}$ the Alfvén speed based on the azimuthal component B_ϕ of the field. This is independent of the poloidal field component, at least for the so-called internal kink modes (which do not disturb the outer boundary of the field, cf. Bateman 1978 for details). For stability analysis and numerical simulations with astrophysical applications see, e.g. Begelman (1998); Appl et al. (2000); Lery et al. (2000); Ouyed et al. (2003); Nakamura & Meier (2004). Based on linear theory, we would predict that the poloidal field component can be ignored for the rate of energy release.

It is not clear, however, that the poloidal component can be ignored for the nonlinear development of the instability, which is what actually determines the energy release. As a way to explore the effect of possible nonlinear stabilization by a poloidal component we compare two cases in the calculations: one with energy release and field decay given by the Alfvén time across the jet ($t_{\rm k}$ above), and one in which this rate is assumed to be reduced by the poloidal component. This mainly affects the early phases of the acceleration of the flow beyond the light cylinder.

We find that kink instability has time to grow in the AGN and XRB cases, dissipating energy in the toroidal component of the magnetic field while accelerating the flow at the same time. The dissipation of magnetic energy is almost complete and fast in the case of AGN jets, so that on parsec scales the flow has become kinetic energy dominated, in agreement with current interpretations of the observations (e.g. Sikora et al. 2005, where the possible effects of magnetic dissipation are also discussed briefly).

The DC model with kink instability also produces significant flow acceleration in the GRB case, but conversion of the Poynting flux is less effective than the AC model in this case.

The structure of the paper is as follows. In Sec. 2 we discuss MHD instabilities in jets and focus on the kink instability and its growth rate. The model is described in Sec. 3 including the assumptions, the dynamical equations and the parameters at the base of the flow. In Sec. 4, we apply the model to the case of AGN jets and GRBs, while the last two Sections present the discussion and conclusions.

2. The kink instability

Magnetized outflows are subject to a variety of instabilities. These can be classified as pressure driven, Kelvin-Helmholtz and current driven instabilities (see, e.g., Kadomtsev 1966; Bateman 1978). Pressure driven instabilities (Kersalé et al. 2000; Longaretti 2003) are related to the interplay between the gas pressure and the curvature of magnetic field lines. They are relevant close to the launching region of the outflows and may be important as long as the outflow is still subsonic. Kelvin-Helmholtz (KH) instabilities (Ray 1981; Ferrari et al. 1981; Bodo et al. 1989; Hardee & Rosen 1999) arise from velocity gradients in the flow and may be important in the shearing layer between the outflow and the external medium. KH instabilities have been extensively studied and become strongest in the region beyond the Alfvén point but still within the fast magnetosonic point. Current driven (CD; Eichler 1993; Spruit et al. 1997; Begelman 1998; Lyubarskii 1999; Appl et al. 2000) instabilities have received much less attention but are the most relevant ones for Poynting-flux dominated outflows, since they can convert the bulk Poynting flux into radiation and kinetic energy of the flow (for the role of CD instabilities in an electromagnetic model for GRBs see Lyutikov & Blandford 2003). Among the CD instabilities, the m =1 kink instability is generally the most effective. In this work, we focus on the effect of the kink instability on the dynamics of these outflows.

2.1. The growth rate of the instability

While magnetized outflows can be accelerated "centrifugally" by large scale poloidal fields (Blandford & Payne 1982; Sakurai 1985, 1987), at the radius of the light-cylinder inertial forces become significant and the magnetic field cannot force corotation. At this radius the strength of the toroidal and the poloidal components are

comparable. Further out, the induction equation dictates that, within ideal MHD, the toroidal component dominates over the poloidal one since the strength of the former scales as $1/r$ while that of the latter as $1/r^2$. This magnetic configuration of a strongly wound-up magnetic field like this is known, however, to be highly unstable to the kink $m = 1$ mode from tokamak experiments (see, e.g., Bateman 1978). Linear stability analysis has shown that the growth time of the instability is given by the Alfvén crossing time across the outflow in a frame comoving with it (Begelman 1998; Appl et al. 2000).

The study of the non-linear evolution of the instability demands three dimensional relativistic MHD simulations over many decades of radii and it is, therefore, not surprising that the issue is not settled. Lery et al. (2000) and Baty & Keppens (2002) argued in favor of the dynamical importance of the instability in reorganizing the magnetic configuration inside the jet. It has been argued, however, that the jet creates a "backbone" of strong poloidal field which slows down the development of instabilities (Ouyed et al. 2003; Nakamura & Meier 2004). In view of these works and since the growth rate of the instability is important for this study, we consider two alternatives for the non-linear stage of the instability. In the first case, the instability proceeds at the Alfvén crossing time across the outflow (as suggested by linear stability analysis) and rearranges the magnetic field configuration to a more chaotic one. In this case the instability time scale is given by the expression (in the central engine frame)

$$t_{\rm k} = \frac{r\theta\gamma}{v_{{\rm A},\phi}}. \qquad (1)$$

We will refer to this as the "fast kink" case.

For the second case, we reduce the dissipation rate by a suitable (but arbitrary) function of the poloidal-to-toroidal field ratio.

$$t_{\rm k} = \frac{r\theta\gamma}{v_{{\rm A},\phi}} e^{B_p^{\rm co}/B_\phi^{\rm co}}. \qquad (2)$$

We will refer to this as the "slow kink" case. This recipe is meant only as a means to explore the possible effect that the poloidal field component could have on the net acceleration of the flow, if it affects the dissipation rate, and is not meant to be quantitative. Numerical simulations of the instability would be needed to determine which of these prescriptions (if any) of the growth time scale is close in describing its non-linear development (see also Section 5). In the last expressions, $B_\phi^{\rm co}$, $B_p^{\rm co}$, are the toroidal and the poloidal components of the magnetic field as measured by an observer comoving with the flow, θ is the jet opening angle, γ is the bulk Lorentz factor of the flow and $v_{{\rm A},\phi}$ is the ϕ component of the Alfvén speed given by

$$v_{{\rm A},\phi} = c\frac{u_{{\rm A},\phi}}{\sqrt{1+u_{{\rm A},\phi}^2+u_{\rm A,p}^2}}, \qquad u_{{\rm A},\phi} = \frac{B_\phi^{\rm co}}{(4\pi w)^{1/2}}. \qquad (3)$$

Here, w is the internal enthalpy, to be defined below.

3. The model

A magnetically launched outflow passes through three characteristic points where the speed of the flow equals the speed of slow mode, the poloidal Alfvén wave and the fast mode and are called the slow magnetosonic, the Alfvén and the fast magnetosonic points respectively. For flows where the energy density of the magnetic field dominates that of matter, the Alfvén point lies very close to the light-cylinder

$$R_L = c/\Omega, \qquad (4)$$

where Ω is the angular velocity of the foot point (e.g. Camenzind 1986). At the Alfvén radius most of the centrifugal acceleration has already taken place and the magnetic field cannot force corotation of matter. At this location, the toroidal and the poloidal components of the magnetic field are comparable in magnitude. Further out, the flow passes through the fast magnetosonic point at a distance $\sim$ a few $\rm R_L$ (Sakurai 1985; Li et al. 1992; Beskin et al. 1998). At the location of the fast magnetosonic point the speed of the four-velocity of the flow equals $\sim \mu^{1/3}$, where μ is the Michel magnetization parameter (i.e., the energy flux per unit rest mass; Michel 1969). For Poynting-flux dominated flows (i.e., $\mu \gg 1$), most of the energy is still in magnetic form at this point since the ratio of magnetic to matter energy flux is $\sim \mu^{2/3}$. There is thus a choice between flows with high Lorentz factors (but inefficient conversion of Poynting flux to kinetic energy), or efficient conversion at the price of low terminal Lorentz factors. Better conversion within ideal MHD appears to be hard to achieve except by decollimation of the flow (Li et al. 1992; Begelman and Li 1994, Bogovalov 2001; Daigne and Drenkhahn 2002; but see claims to the contrary by Vlahakis and Konigl 2003a,b; Fendt and Ouyed 2004). Even with such decollimation, the additional acceleration is rather modest (Begelman and Li 1994; Daigne and Drenkhahn 2002).

We set the initial conditions of our calculation at the fast magnetosonic point r_0. To make the problem tractable we make a number of simplifying assumptions. First, we limit ourselves to a *radial*, *static* flow. Evidently, this approach does not allow us to explore the important issue of jet collimation (see, however Section 5.1). Furthermore, the flow is assumed *one-dimensional* by ignoring the structure of the jet in the θ direction. Also, we ignore the azimuthal component of the velocity. This component is not dynamically important beyond the fast magnetosonic point (e.g. Goldreich & Julian 1970) and can be neglected from the dynamic equations. On the other hand, the poloidal component (taken to be radial for simplicity) still has to be taken into account when modeling the effect of the kink instability since it influences its growth timescale [see Eqs. (1), (2)]. These simplifying assumptions minimize the number of the free parameters of the model, allowing us to study the effect of each on the jet dynamics, as will become clear in the next sections.

3.1. Dynamical equations

To determine the characteristics of the flow as a function of radius, one needs the conservation equations for mass, energy and angular momentum. These equations can be brought in the form (if, for the moment, we neglect radiative losses; e.g. Lyutikov 2001; Drenkhahn 2002)

$$\partial_r r^2 \rho u = 0, \tag{5}$$

$$\partial_r r^2 \Big(w\gamma u + \frac{\beta B_\phi^2}{4\pi} \Big) = 0, \tag{6}$$

$$\partial_r r^2 \Big(w u^2 + p + \frac{(1+\beta^2) B_\phi^2}{8\pi} \Big) = 2rp, \tag{7}$$

where $w = \rho c^2 + e + p$ is the proper enthalpy density, e and p are the internal energy and pressure respectively and $u = \gamma\beta$ is the radial four-velocity. We still need to assume an equation of state that will provide a relation between the pressure p and the internal energy. Assuming an ideal gas, we take $p = (\gamma_a - 1)e$, where γ_a is the adiabatic index.

Mass conservation (5) can be integrated to yield mass flux per sterad

$$\dot{M} = r^2 u \rho c, \tag{8}$$

while energy conservation gives the total luminosity per sterad

$$L = w r^2 \gamma u c + \frac{\beta c (r B_\phi)^2}{4\pi}. \tag{9}$$

The first term of the last expression corresponds to the kinetic energy flux and the second to the Poynting flux. A key quantity is the "magnetic content" of the flow which we will refer to as the magnetization parameter σ, defined as the ratio of the radial Poynting to matter energy flux

$$\sigma = \frac{L_{\rm pf}}{L_{\rm kin}} = \frac{B_\phi^2}{4\pi\gamma^2 w}. \tag{10}$$

For a flow to reach large asymptotic Lorentz factors (observations indicate $\gamma \sim 10 - 20$ for quasars, and theoretical arguments arising from the "compactness problem" such as Piran 1999 constrain $\gamma \gtrsim 100$ for GRBs), it must start with a high energy to mass ratio. Within the fireball model for GRBs (Paczyński 1986; Goodman 1986) this means that $e \gg \rho c^2$. In this work, we focus on the opposite limit where most of the energy is initially stored in the magnetic field ($\sigma_0 \gg 1$), while we treat the flow as cold (i.e., $e \lesssim \rho c^2$). Obviously, there can exist an intermediate regime of a "magnetized-fireball" models where both $e/\rho c^2$ and $\sigma_0 \gg 1$ at the base of the flow.

Finally, the strength of the radial component is given by flux conservation by the expression

$$B_r = B_{r,0} \Big(\frac{r_0}{r} \Big)^2. \tag{11}$$

For a flow that is moving radially with a bulk Lorentz factor γ, the expressions that relate the comoving components of the magnetic field to those measured in the central engine frame are

$$B_r^{co} = B_r \tag{12}$$

and

$$B_\phi^{co} = \frac{B_\phi}{\gamma}. \tag{13}$$

3.2. Modeling the kink instability

The set of equations presented in the previous section is not complete. There is one more equation needed to determine the problem at hand, which is the induction equation. For ideal MHD, the induction equation yields $\partial_r \beta r B_\phi = 0$ and can be integrated to give the scaling $B_\phi \propto 1/r$ for relativistic flows. One can immediately see that the Poynting-flux term in equation (9) is approximately constant and no further acceleration of the flow is possible within ideal MHD for a radial flow. This is a result of the fact that the magnetic pressure and tension terms of the Lorentz force almost cancel each other (Begelman & Li 1994).

We argue, however, that when the toroidal component of the magnetic field becomes dynamically dominant the kink instability sets in. The instability drives its energy from B_ϕ^2 on the instability growth time scale. This effect can be crudely modeled by the addition of one sink term on the right hand side of the induction equation following Drenkhahn (2002), Drenkhahn & Spruit (2002)

$$\partial_r \beta r B_\phi = -\frac{r B_\phi}{c t_{\rm k}}. \tag{14}$$

The kink instability time scale is given by the expressions (2) or (1) depending on whether the poloidal component of the magnetic field is assumed to have a stabilizing effect. When the instability sets in, B_ϕ drops faster than $1/r$ and acceleration of the flow is possible at the expense of its magnetic energy.

3.3. Radiative losses

The dynamical equations (6) and (7) are derived under the assumption that no energy or momentum escape from the outflow. This is accurate when the instability releases energy in the optically thick region of the flow. On the the other hand, in the optically thin regime energy and momentum may be transfered into the radiative form that escapes and does not interact with matter. Let Λ be the emissivity of the medium in the comoving frame, that is, the energy that is radiated away per unit time and per unit volume. If the emission is isotropic in the comoving frame the energy and momentum Eqs. (6), (7) including the radiative loss terms are (Königl & Granot 2002)

$$\partial_r r^2 \left(w\gamma u + \frac{\beta B_\phi^2}{4\pi} \right) = -r^2 \Gamma \frac{\Lambda}{c}\ , \tag{15}$$

$$\partial_r r^2 \left(w u^2 + p + \big(1+\beta^2\big) \frac{B_\phi^2}{8\pi} \right) = 2rp - r^2 u \frac{\Lambda}{c}. \tag{16}$$

The importance of the cooling term depends on the cooling time scale. If it is short compared to the expansion

time scale, the matter stays cold during the dissipation process. In this limit, all the dissipated energy is locally radiated away. The dissipative processes that appear in the non-linear stage of the instability are poorly understood. It could be the case that the released energy leads to fast moving particles (i.e. electrons and ions) and/or to Alfvén turbulence (Thompson 1994). Synchrotron emission is a plausible fast cooling process for the electrons. It is particularly effective in our model, because the magnetic field strengths are high in a Poynting flux dominated outflow. Ions, however, are, due to their higher masses, much less efficient radiators.

The form of this cooling term we assume here is

$$\Lambda = \kappa \frac{ecu}{r} \tag{17}$$

where k is an adjustable cooling length parameter. The cooling length is the distance by which the matter travels outward while the internal energy e is lost. When $\kappa \gg 1$ the cooling length is very short, only a small fraction of the expansion length scale r and thus qualifies for the description of a fast cooling flow. This, in more physical terms, corresponds to the case where most of the energy is dissipated to fast moving (and therefore fast cooling) electrons. On the other hand, setting $\kappa \ll 1$, the cooling length is much longer than the expansion length and most of the energy stays in the flow leading to more efficient adiabatic expansion. This is the case when the dissipated energy is mostly shared among the ions.

3.4. Initial conditions, model parameters

The characteristics of the flow are determined when a number of quantities are specified at the fast magnetosonic point r_0 which is taken to be $\sim$ a few times the light cylinder radius (Sakurai 1985; Begelman et al. 1994; Beskin et al. 1998), or expressed in terms of the gravitational radius $r_g = GM/c^2$ of the central engine $r_0 \sim 100 r_g$. These quantities are the initial magnetization σ_0, the luminosity L, the opening angle θ, the ratio $B_{r,0}/B_{\phi,0}$ and the cooling length scale κ. The quantities one has to solve for so as to determine the characteristics of the flow are ρ, e, u and B_ϕ as functions or radius r. This is done by integrating numerically the mass, energy, momentum conservation equations and the modified induction equation. The parameters of the model determine the initial values of ρ, e, u and B_ϕ at r_0.

The initial four-velocity for our calculations is assumed to be

$$u_0 = \mu^{1/3} = \sqrt{\sigma_0}, \tag{18}$$

in accordance with previous studies (Michel 1967; Goldreich & Julian 1970; Camenzind 1986; Beskin et al. 1998) which show that at the fast point the ratio of Poynting to kinetic flux is $\mu^{2/3}$. The flow is assumed to be cold at r_0, i.e. $e = 0$ and using the previous expression with Eqs. (9), (10) one finds for ρ_0 and $B_{\phi,0}$

$$\rho_0 = \frac{L}{r_0^2 c^3 \sqrt{\sigma_0(\sigma_0+1)^3}} \tag{19}$$

and

$$B_{\phi,0} = \frac{4\pi}{r_0}\Big(\frac{\sigma_0}{\sigma_0+1}\Big)^{1/4}\sqrt{\frac{L}{c}}. \tag{20}$$

The role of the different model parameters becomes clear in the next section where the model is applied to the case of AGN jets and GRBs. Out of the free parameters of the model, σ_0 and θ are of special importance. The magnetization σ_0 determines the "magnetic dominance" of the flow, i.e., the speed of the flow at the fast magnetosonic point and at a large distance from the central engine. On the other hand, the opening angle θ is directly related to the growth rate of the instability [see Eqs. (1), (2)]. The instability has enough time to grow if it is faster than the expansion time r/c. The ratio of the two time scales at the base of the flow is (using prescription (1) for the time scale of the kink instability)

$$t_k/t_{exp} = \frac{\theta\gamma_0 c}{v_{A,\phi}} \simeq \frac{\theta\sqrt{\sigma_0}c}{v_{A,\phi}}. \tag{21}$$

If $t_k/t_{exp} \gg 1$, the kink instability does not have enough time to grow and the evolution is close to that predicted by ideal MHD (where not much acceleration takes place). On the other hand, if $t_k/t_{exp} \ll 1$, the instability grows for many e-foldings and turns almost all the magnetic energy in the flow into radiation and kinetic flux. Keeping the opening angle fixed, this happens much more efficiently in lower σ_0 flows (provided that $\sigma_0 \gtrsim 1$ so that the Alfvén speed is a significant fraction of the speed of light). We return to this point in the next sections.

4. Applications

Although at first sight different, jets in AGNs (and microquasars) and GRBs probably have central engines of similar characteristics. AGN jets are launched in the inner regions of magnetized accretion disks (Blandford & Payne 1982), or drive their power by magnetic fields that are threading the ergosphere of a rotating black hole (Blandford & Znajek 1977). In the case of GRBs, the same central engine may be at work, or the energy is tapped by a millisecond magnetar (Usov 1992; Kluźniak & Ruderman 1998; Spruit 1999). In all of these situations, strong magnetic fields play an important role and most of the energy is released in the form of Poynting flux. [1]

[1] An exception is the possibility of creation of a fireball by neutrino-antineutrino annihilation at the poles of a hyperaccreting compact object (Jaroszyński 1993; Mochkovitch et al. 1993), an idea applied to long bursts within the collapsar scenario (Woosley 1993; MacFadyen & Woosley 1999) and short bursts within the binary merger scenario (Blinnikov et al. 1984; Eichler et al. 1989; Janka et al. 1999; Aloy et al. 2005)

All the above scenarios may give rise to magnetized outflows, whose evolution depends, to a large extent, on the dominance of the magnetic energy or on the ratio of the Poynting-flux to matter energy flux at the base of the flow. By varying this ratio, one can apply the model to jets in both the cases of GRBs and AGNs.

4.1. AGN jets

Relativistic jets are commonly observed in AGNs to have bulk Lorentz factors in the range $\gamma \sim 10 - 20$. Such terminal Lorentz factors can be achieved for the ratio σ_0 of Poynting to matter energy flux of the order of several at the fast magnetosonic Point r_0. The location of the fast point is most likely at a few light cylinder radii (e.g. Sakurai 1985; Camenzind 1986) and is taken to be $100r_g$.

Actually, σ_0 is a very important parameter of the flow. Its effect on the acceleration of the flow is clearly seen in Fig. 1, where the bulk Lorentz factor is plotted as a function radius r for different σ_0. The rest of the parameters have the values $\theta = 10^o$, $B_{r,0}/B_{\phi,0} = 0.5$, while the energy released by the instability is assumed to be locally radiated away (this is done by taking the "cooling length" parameter $\kappa \gg 1$). The results do not depend on the luminosity L of the flow in the case of AGN jets, while r_0 sets the scale of the problem (since it is the only length scale) which means that the results can be trivially rescaled in the case of a different choice of r_0.

The solid lines in Fig. 1 correspond to the case where Eq. (1) is used for the timescale of the kink instability (i.e., the fast kink case) and the dashed lines to the case where the instability is slowed down by the poloidal component of the magnetic field and the time scale is given by Eq. (2) (i.e., the slow kink case). From Fig. 1, one can see that the instability acts quickly and accelerates the flow within 1-2 orders of magnitude in distance from the location of the fast magnetosonic point. The acceleration is faster in the "fast kink" case and much more gradual in the "slow kink" one. This is due to the fact that close to the base of the flow the ratio $B_r^{co}/B_\phi^{co} = \gamma B_r/B_\phi \sim 1$ and the instability is slowed down [see Eq. (2)]. Further out, however, the toroidal component of the field also dominates in the frame comoving with the flow and the instability proceeds faster. At larger distances, practically all the magnetic energy has been dissipated and the terminal Lorentz factors are very similar in the slow and fast kink cases.

The acceleration of the flow and the terminal Lorentz factor depend also on what fraction of the instability-released energy is radiated away. If the dissipative processes that appear in the non-linear regime of the evolution of the instability lead to fast moving electrons, then it is easy to check that they will radiate away most of this energy through synchrotron (and/or inverse Compton) radiation on a time scale much shorter than the expansion timescale. If, on the other hand, most of the energy is dissipated to the ions, then most of it stays in the system as internal energy and accelerates the flow further.

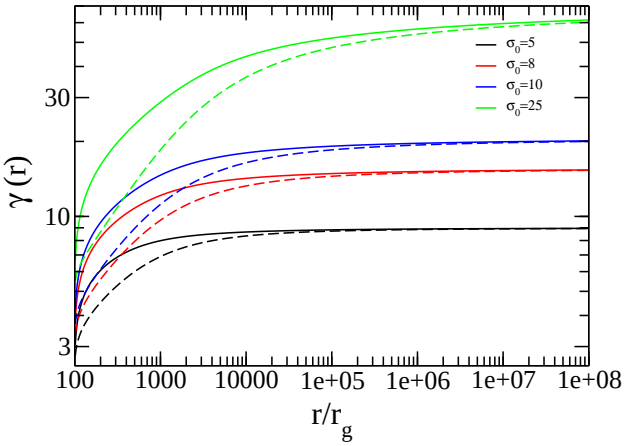

Fig. 1. The bulk Lorentz factor of the flow as a function of radius for different values of σ_0. The black, red, blue and green curves correspond to $\sigma = 5$, 8, 10 and 25 respectively. The solid curves correspond to the case where Eq. (1) is used for the instability growth time scale (fast kink) and the dashed to the one where Eq. (2) is used (slow kink case).

To keep this study fairly general, we have calculated the bulk Lorentz factor of the flow in the two extreme cases. In the "fast cooling" case, all the released energy is radiated away very efficiently, while in the "slow cooling" case, the energy is assumed to stay in the flow (practically this means that we set the cooling length parameter $\kappa \ll 1$).

In Fig. 2, the bulk Lorentz factor of the flow is plotted for $\sigma_0 = 8$. The red curves correspond to the "fast cooling" case and the black to the "slow cooling" one. The asymptotic bulk Lorentz factor differs substantially in these two cases, showing that a large fraction of the energy of the flow can in principle be radiated away due to the instability-related dissipative processes. Furthermore, the acceleration of the flow depends on the jet opening angle and is faster for narrower jets (see green curves in Fig. 2). This is expected, since for a narrower opening angle, the Alfvén crossing time across the jet is shorter and so is the instability growth timescale.

Another quantity of special interest is the Poynting to matter energy flux ratio σ as a function of radius. While the flow is initially moderately Poynting flux dominated, the σ drops rapidly as a function of distance and the flow is matter-dominated at distances $r \gtrsim 10^3 r_g$ independently of the prescription of the instability or the cooling timescales. Far enough from the fast magnetosonic point, practically all the magnetic energy has been transfered to the matter, and the bulk Lorentz factor saturates.

The thick lines in Fig. 3 show the ratio of the radial to the toroidal components of the magnetic field. This ratio drops rapidly as a function of distance showing that $B_\phi \gg B_r$. So, despite the fact that the instability grows

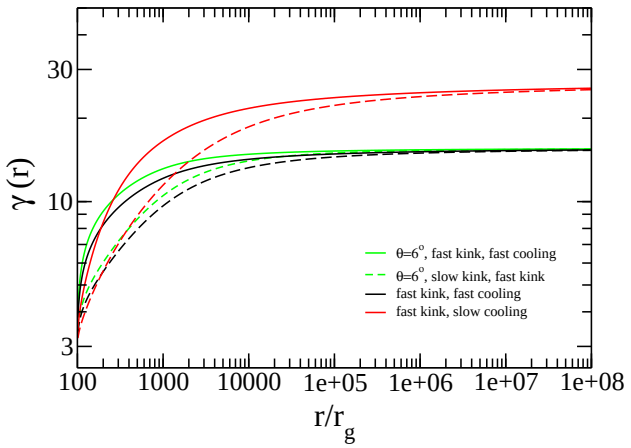

Fig. 2. The bulk Lorentz factor dependence on the cooling efficiency of the flow and jet opening angles. The solid curves correspond to the fast kink case while the dashed to the slow kink one. The black, red and green curves correspond to fast cooling, slow cooling and jet opening angle of 6^o respectively.

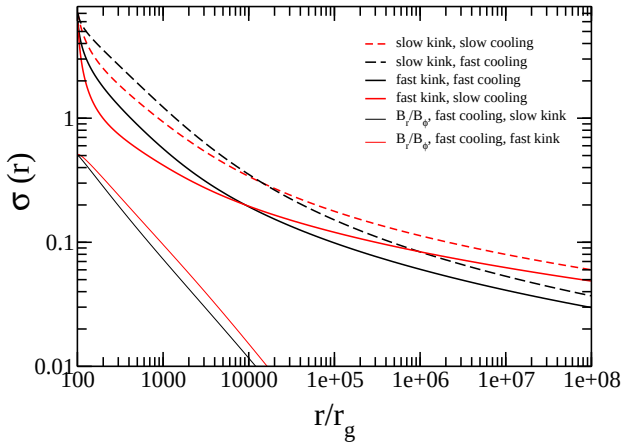

Fig. 3. The dependence of the magnetization parameter on the radius for the different prescriptions of radiative cooling and the instability timescale. Notice that the flow becomes matter-dominated at distances greater than $\sim 10r_0$. The thick lines show the ratio of the radial to the toroidal components of the magnetic field in the flow. The dominant component is clearly the toroidal one.

quickly from the toroidal component of the magnetic field, this component still dominates over the radial one.

Having solved for the dynamics of the flow predicted by our modeling of the kink instability, we turn to the implications of these findings for observations of AGN jets. One highly debated issue is whether the AGN jets are Poynting-flux dominated on pc and kpc scales or not. The case-dependent arguments are reviewed in Sikora et al. (2005), where it is shown that there is no strong observational reason to assume Poynting-flux dominated jets on scales larger than a few pc and that the observed emission on these scales can be understood as energy dissipated in shocks internally in the flow (Sikora et al. 1994; Spada et al. 2001) or due to interaction of the flow with the external medium.

Our model predicts that most of the energy is in the form of kinetic flux at distances say $\gtrsim 10^3 - 10^4 r_g \simeq 10^{17} - 10^{18} m_9$ cm, where m_9 is a black hole of 10^9 solar masses. So, on pc scales the magnetic fields are dynamically insignificant, in agreement with observations. Further information on the dynamics of AGN jets comes from the shortest variability timescale in the optical and gamma-ray bands in blazars. This timescale can be as short as a few days, indicating that most of the non-thermal radiation comes from a compact region of size $R \lesssim 10^{17}$ cm (the so-called blazar zone). On the other hand, polarimetry measurements of the variable optical, infrared and mm radiation are consistent with a toroidal magnetic field geometry on sub-pc scales (e.g. Impey et al. 1991; Gabuzda & Sitko 1994; Nartallo et al. 1998).

Since most of the magnetic energy is dissipated on these scales, it is quite probable that the observed radiation is the result of the instability-released energy, provided that the dissipative processes lead to wide enough particle distributions (see also Sikora et al. 2005). However, one cannot exclude the possibility that, within this model, the "blazar zone" emission is a result of internal shocks. On scales of 10^{17} cm, the magnetization parameter of the flow is of the order of unity and it is interesting to study the outcome of internal shocks of moderately magnetized plasma. The rich blazar phenomenology may indicate that both these mechanisms (i.e. magnetic dissipation and internal shocks) are at work.

Further constraints on where the acceleration of the flow takes place come from the lack of bulk-flow Comptonization features in the soft X-rays. This indicates that $\gamma \lesssim 10$ at $\sim 10^3 r_g$ (Begelman & Sikora 1987; Moderski et al. 2003). This shows that the acceleration process is still going on at these distances. In view of our results, this could in principle rule out the "fast kink" case since the acceleration appears to be too fast and $\gamma \sim 10$ already at $\sim 300 r_g$ or so. At this point, however, the uncertainties in the model are too high to make a strong statement on this issue. If, for example, the fast point is located at a factor of, say, ~ 3 larger distance, our results are compatible with the lack of soft X-ray features. Numerical simulations of the instability are needed so that these issues can be settled (see also discussion in Sect. 5).

4.2. Gamma-ray bursts

The analysis we follow so as to apply the model to GRBs is very similar to that described in the previous sections. The only new ingredient that has to be added is related to the very high luminosities that characterize the GRB jets. As a result, the inner part of the flow is optically

thick to electron scattering and matter and radiation are closely coupled. At the photospheric radius the optical depth drops to unity and further out the flow is optically thin. So, the high luminosity introduces a new length scale to the problem that has to be treated in a special way described in the next section.

4.2.1. Below and above the photosphere

At the photosphere, the equation of state changes from one dominated by radiation to one dominated by the gas pressure. To connect the two, the radiation emitted at the photosphere has to be taken into account. The amount of energy involved can be substantial, and appears as an (approximate) black body component in the GRB spectrum. It depends on the temperature of the photosphere.

The temperature at the photosphere is $kT \ll m_e c^2$ for all parameter values used so that pairs can be neglected. The photosphere is then simply defined as (e.g. Abramowicz et al. 1991)

$$\int_{r_{\rm ph}}^{\infty} (1-\beta)\gamma\kappa_{es}\rho {\rm dr} \equiv 1, \tag{22}$$

where κ_{es} is the electron scattering opacity. The dynamics of the flow depend on the location of the photosphere since above the photosphere all the dissipated energy can in principle be radiated away while this is not possible at large optical depths. To solve Eq. (22) for $r_{\rm ph}$, we have followed an iterative method. First, we guess a value for $r_{\rm ph}$ and integrate the dynamical equations assuming no radiative losses below the photosphere and fast cooling above it. Then we calculate the optical depth τ from r_{ph} to ∞ and, if τ differs from unity by more than a threshold value (~ 0.01 in these calculations), a new guess for $r_{\rm ph}$ is made. The procedure continues until the definition (22) is satisfied.

At the photosphere one has to subtract the energy and momentum carried away by the decoupled radiation. To calculate these quantities one needs the temperature at the photosphere. The dimensionless temperature $\theta = kT/(m_e c^2)$ in the optically thick region is given by the solution of

$$e = 3\frac{m_{\rm e}}{m_{\rm p}}\rho c^2\theta + \frac{8\pi^5}{15}\frac{m_{\rm e}c^2}{\lambda_e^3}\theta^4 \tag{23}$$

where λ_e is the electron Compton wave length. The terms in (23) correspond to the matter and radiation energy density. From this solution, we have also found that the internal energy is always dominated by radiation (for parameters relevant for GRBs), so we take $\gamma_a = 4/3$ below the photosphere.

At the photosphere we calculate the temperature $\theta_{\rm ph}$ and subtract the radiation energy density of a black body

$$e_{\rm bb} = \frac{8\pi^5}{15}\frac{m_{\rm e}c^2}{\lambda_e^3}\theta_{\rm ph}^4 \tag{24}$$

from the total energy density: $e \equiv e - e_{\rm bb}$. The integration proceeds with an adiabatic index of $\gamma_a = 5/3$. The temperature $\theta_{\rm ph}$ is the temperature of the emitted black-body radiation which has a luminosity per sterad of

$$L_{\rm ph} = r_{\rm ph}^2 \frac{4}{3} e_{\rm bb} u_{\rm ph} \gamma_{\rm ph} c \quad \text{for } r \geq r_{\rm ph}. \tag{25}$$

The integration continues until large distances from the source (taken as 10^{16} cm, where the afterglow phase starts). There, the radiative luminosity is determined by

$$L_{\rm rad} = L - L_{\rm pf} - L_{\rm mat}\ . \tag{26}$$

This means that the radiative luminosity is the sum of the photospheric luminosity plus the component coming from the instability-released energy above the photosphere. The role of the photospheric component and its connection to the observed spectral peaks of the GRB prompt emission in internal shock and slow dissipation models (like this one) has been studied in a number of recent papers (Ryde 2005; Rees & Mészáros 2005; Pe'er et al. 2005).

4.2.2. Results

Following the procedure described in the previous section, we have calculated the bulk Lorentz factor of the flow for different values of σ_0 at the base of the flow and for the two prescriptions for the timescale of the kink instability [Eqs. (1), (2)]. The fast magnetosonic point is set to $R_0 = 10^8$ cm, the jet opening angle to $\theta = 10^o$, the initial ratio $B_{r,0}/B_{\phi,0} = 0.5$ and the luminosity of the flow $L = 10^{51}$ erg/sec $\cdot$ sterad.

The results are given in Fig. 4, where it is shown that the flow reaches terminal Lorentz factors $\gamma \gtrsim 100$ for $\sigma_0 \gtrsim 30$. The solid curves correspond to the case where the timescale for the kink instability is given by Eq. (1) (fast kink case) and the dashed to the case where Eq. (2) is used for the timescale of the growth of the instability (slow kink case). Notice that the initial acceleration of the flow differs in the two cases, being much faster in the fast kink case. This is expected since this case is characterized by rapid dissipation of magnetic energy and acceleration from the base of the flow, while in the slow kink case the non-negligible poloidal component of the magnetic field close to r_0 slows down the instability. The terminal Lorentz factors are, however, similar in the two cases. Notice also that there is a discontinuity in the slope of the curves $\gamma(r)$ at the location of the photosphere which is a result of our simplistic approach (for details see previous section).

A second key parameter of the model is the opening angle of the jet. For smaller opening angles, the instability timescale becomes shorter and the flow is accelerated faster and to higher terminal Lorentz factors as is shown in Fig. 5. This implies that for smaller opening angles, more magnetic energy is dissipated and the flow is less strongly magnetized at large distances. This is clearly shown in Fig. 6, where the Poynting to matter energy flux ratio is plotted as a function of radius r (compare the thin curve with the thick black dashed curves). Notice that the

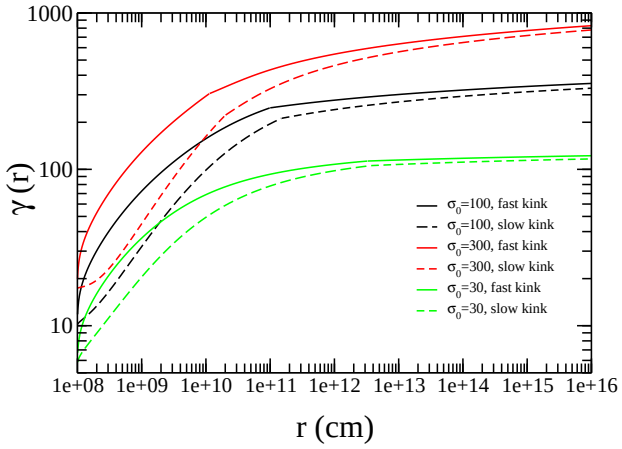

Fig. 4. The bulk Lorentz factor of the flow for different σ_0 and for the fast and slow kink case. Notice that larger values for σ_0 result in faster outflows.

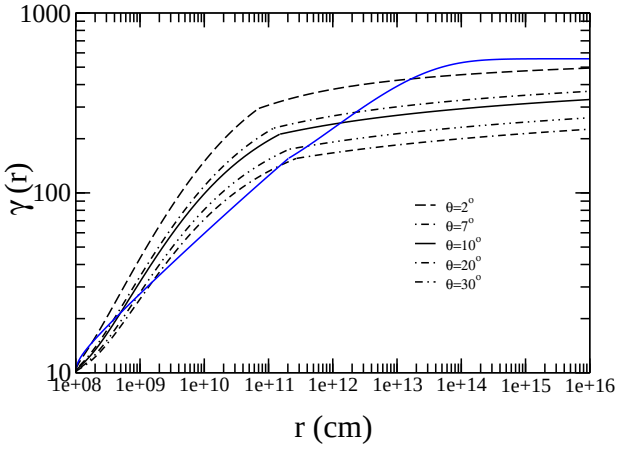

Fig. 5. The bulk Lorentz factor of the flow for different jet opening angles θ. For smaller opening angles, the terminal Lorentz factors of the flow become larger because of more efficient dissipation of the magnetic energy. The blue curve corresponds to the non-axisymmetric case studied by Drenkhahn & Spruit (2002).

σ(r) curves are discontinuous at the location of the photosphere. This is caused by our simplified treatment at the location of the photosphere, where we subtract the energy density of the radiation field (see previous section) and reduce the internal enthalpy of the flow, increasing the ratio of Poynting to matter energy flux. More detailed radiative transfer models of the transition from optically thick to optically thin condition, predict a rather sharp transition which indicates that our simple approach does not introduce large errors.

In Figs. 5 and 6 we have also plotted (see blue curves) the bulk Lorentz factor and the magnetization σ as functions of r for the "typical values" of the parameters of the model proposed by Drenkhahn & Spruit (2002; the "AC" flow). In the context of that model the magnetic field lines change direction on small scales and magnetic reconnection dissipates magnetic energy and accelerates the flow. Notice that the non-axisymmetric model predicts more gradual acceleration and rather higher terminal Lorentz factors (for the same initial magnetization of the flow) than the current model. Furthermore, it is characterized by efficient dissipation of the Poynting flux, resulting in negligible magnetization sufficiently far from the central engine (at least in the case where the non-decayable axisymmetric component is negligible).

One important point deduced from Fig. 6 is that, for $\sigma_0 \gtrsim 100$, the flow remains Poynting-flux dominated even at large distances away from the source where deceleration of the outflow because of its interaction with the interstellar medium or the stellar wind is expected, which means that the instability is not fast enough to convert most of the magnetic energy into bulk motion of matter. Afterglow observations can in principle probe to the magnetic content of the ejecta through early observations of the reverse shock emission (Fan et al. 2002; Zhang et al. 2003; Kumar & Panaitescu 2003). Modeling of the forward and reverse shock emission in cases where quick follow ups were possible suggests the existence of frozen-in magnetic fields in the ejecta (Kumar & Panaitescu 2003) that are dynamically important, with $\sigma \gtrsim 0.1$ (Zhang & Kobayashi 2005). Rapid follow-ups in the X-rays, UV and optical are now possible thanks to Swift satellite and ground based telescopes and can test our model which predicts a magnetization parameter of the order of unity for the outflowing material in the afterglow region. The XRT instrument on board Swift has already provided several early X-ray afterglows (e.g. Tagliaferri et al. 2005; Campana et al. 2005; Burrows et al. 2005). Many of these observations indicate a slow fading component at times $10^2 - 10^4$ sec after the GRB trigger (Nowsek et al. 2005; Zhang et al. 2005; Panaitescu et al. 2005) which may be expected by the deceleration of ejecta with $\sigma \gtrsim 1$ (Zhang & Kobayashi 2005; Zhang et al. 2005) in agreement with our model predictions.

The ratio σ is even higher for the range of distances $r \sim 10^{13} - 10^{15}$ cm where internal shocks are expected to happen in the internal shock scenario for GRBs (Rees & Mészáros 1994; Piran 1999) and is expected the reduce their radiative efficiency. However, allowing for non-ideal MHD effects in the shocked region, Fan et al. (2004) show that the radiative efficiency of $\sigma \sim 1$ plasma may not be much lower than the $\sigma = 0$ case. On the other hand, since the efficiency of internal shocks to convert kinetic energy into gamma rays is already low (typically of the order of a few percent; Panaitescu et al. 1999; Kumar 1999) and observations indicate much higher radiative efficiency (Panaitescu & Kumar 2002; Lloyd & Zhang 2004), we investigate the possibility that the energy released by the instability powers the prompt gamma-ray emission.

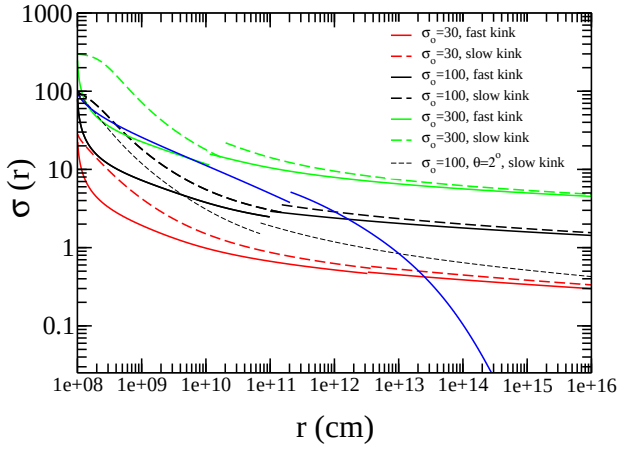

Fig. 6. The magnetization $\sigma(r)$ of the flow as a function of distance for different σ_0 and jet opening angles. Keeping $\theta = 10^o$, the jet is still magnetically dominated at large distance from the source for $\sigma_0 \gtrsim 100$. Smaller jet opening angles lead to lower values of σ_∞. The blue curve corresponds to the non-axisymmetric case studied by Drenkhahn & Spruit (2002). The discontinuity at the location of the photospheric radius is a result of the subtraction of the radiation energy density from the internal energy of the flow.

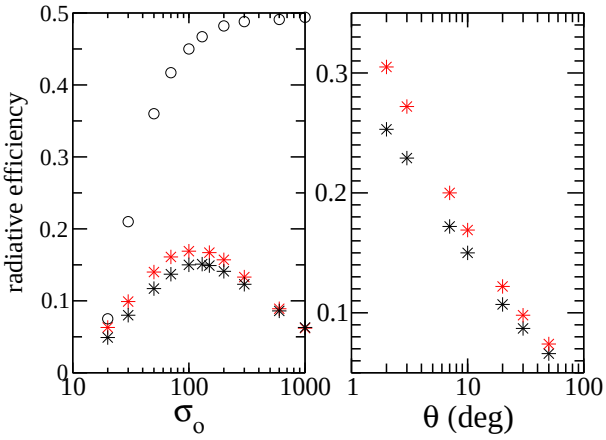

Fig. 7. The radiative efficiency of the flow, defined as the ratio of the radiated luminosity over the luminosity of the flow for different σ_0 and θ. The black and red stars correspond to the fast kink and slow kink cases respectively. For opening angles of $\sim 6^o$ (in accordance with the values deduced by achromatic breaks of the afterglows) the efficiency reaches values of $\sim 20\%$. The circles correspond to the non-axisymmetric case studied by Drenkhahn & Spruit (2002).

In Fig. 7, we plot the radiative efficiency -defined as the radiated luminosity $L_{\rm rad}$ divided by the flow luminosity L- for different values of σ_0 and θ. Fixing the angle θ to 10^o, one can see that the radiative efficiency peaks at $\sim 16\%$ for $\sigma_0 \sim 100$. For smaller values of σ_0, most of the magnetic energy is dissipated below the photosphere and is lost to adiabatic expansion, resulting in lower radiative efficiencies. For larger values of σ_0, the flow remains magnetically dominated at all radii, keeping the radiative efficiency lower. Furthermore, the "slow kink" case has rather higher efficiencies and this comes from the fact that dissipation happens at larger radii and therefore in optically thin environments. So, the model can have large radiative efficiencies for $\sigma_0 \sim 10 - 500$. Notice that one also needs $\sigma_0 \gtrsim 30$ to overcome the "compactness problem" (e.g. Piran 1999).

Fixing $\sigma_0 = 100$, one can now calculate the radiative efficiency for different opening angles of the flow. Smaller opening angles result in more magnetic energy dissipated (by shortening the instability timescale) and therefore to smaller values of Poynting to matter flux at large distances. This also means that more energy is radiated away. Although very model dependent, the opening angles of the GRB jets can be estimated by the achromatic breaks of the afterglow lightcurves (Rhoads 1997, Sari et al. 1999). For $\theta \sim 6^o$ (a value typically inferred), the efficiency is quite high and of the order of 20%.

In Fig. 7, the radiative efficiency of the non-axisymmetric model (Drenkhahn & Spruit 2002) is also shown for different values of σ_0. The non-axisymmetric model can have a higher radiative efficiency which is close to $\sim 50\%$ for $\sigma_0 \gtrsim 100$ (See also Giannios & Spruit 2005 for more detailed study on the spectra expected from this model).

5. Discussion

This work suggests that the kink instability plays a significant role in the dynamics of magnetized outflows. The instability sets in once the toroidal component of the magnetic field becomes dominant and drives its energy by B_ϕ on a short time scale. The energy dissipated by the instability accelerates the flow and turns it into kinetic flux dominated flow for AGN jets at distance $\gtrsim 1000 r_g$ and to moderately magnetized flow for GRB jets in the the afterglow region. If the dissipated magnetic energy is transferred to fast moving electrons with wide enough energy distribution, then it can power the blazar zone emission and the prompt GRB emission with high radiative efficiency.

These results have been compared with those that are predicted by other dissipative models (Coroniti 1990; Spruit et al. 2001; Lyubarsky & Kirk 2001; Drenkhahn 2002; Drenkhahn & Spruit 2002). According to these models, if the magnetic field lines change direction on small scales, magnetic energy can be dissipated through reconnection processes. Drenkhahn (2002) and Drenkhahn & Spruit (2002) applied this idea to GRB outflows and showed that efficient acceleration and radiation (as high as 50%) is possible. In the context of this model, most of

the magnetic energy is dissipated, resulting in kinetic flux dominated flows at large distances where the flow starts to be decelerated by the external medium. On the other hand, our model predicts moderately magnetized ejecta at this region. Since the initial phase of the afterglow emission depends on the magnetic content of the ejecta (e.g. Lyutikov 2005), these models make different predictions about this phase and can be tested against observations.

This study assumes a radial flow and although this allowed us to minimize the number of free parameters and clarify the role of each of them, it nevertheless leaves a number of issues unsettled. Two important issues are these of jet collimation and of the non-linear evolution of the kink instability. We discuss these issues in the next subsections.

5.1. Collimation

The collimation of MHD outflows is usually believed to take place in the trans-Alfvénic region because of the "hoop stress" exerted by the toroidal component of the magnetic field. One issue that arises is whether the same mechanism is at work in the case where the kink instability sets in and reduces the strength of B_ϕ. Our one dimensional approach cannot settle this question; 2-D calculations would be needed if the instability is parametrized as in the present models. Time dependent, 3-D simulations will be needed if the effects of the instability are to be included realistically, since the relevant ones are nonaxisymmetric. Collimation of the flow can be achieved by its interaction with the environment. This may be the collapsing star in the context of gamma-ray bursts (Woosley 1993) or a large scale poloidal field in the case of AGN jets (Spruit et al. 1997). Another interesting possibility is that small scale toroidal fields (probably a result of the development of the instability) can lead to flow collimation under certain conditions (Li 2002).

5.2. The non-linear evolution of the instability

The linear evolution of the kink instability is rather well understood and has been studied by linearizing the MHD equations by a number of authors (e.g. Begelman 1998; Appl et al. 2000), which shows that the instability grows on the Alfvén crossing time across the jet. The non-linear evolution of the instability is an issue that cannot be solved with analytical tools and 3-dimensional RMHD simulations that cover many decades of radii are needed to settle this issue. Preliminary numerical investigations have been done (e.g. Lery et al. 2000; Ouyed et al. 2003; Nakamura & Meier 2004) which indicate that the kink instability is an internal mode that does not disrupt the jet. On the other hand, whether it is able to rearrange the magnetic field configuration internally in the flow on the short timescale implied by linear stability analysis is still not clear.

Some intuition on this issue can be gained by this study. We have tried two different prescriptions for the instability growth time scale, the second of which accounts for its possible slowing down because of a strong poloidal "backbone" in the core on the jet (Ouyed et al. 2003). A non-negligible poloidal component can slow down the initial growth of the instability; eventually it grows in a conical jet. This occurs because as the jet expands, the B_ϕ and B_p scale as $1/r$ and $1/r^2$ respectively so as to satisfy the induction equation. This means that the toroidal component dominates the poloidal at some point and the instability sets in. A study that assumes a cylindrical jet, on the other hand, will not deal with the $B_\phi \gg B_p$ situation. Since the observed jets do expand laterally (despite their strong collimation) by many orders in radius from their launching region to their termination shock, we believe that it is important for numerical investigations of the role of kink instability to allow for jet expansion to reveal the characteristics of the non-linear development of the instability.

5.3. More realistic models

The limitations of the calculations presented here are obvious from the parameterizations used. One may wonder to what extent these can be overcome in numerical simulations. Since the most relevant instabilities are nonaxisymmetric, such simulations have to be 3-dimensional. The computational expense of 3D MHD simulations puts strong limitations on the kind of calculations that can be done, and the realism of the conclusions that can be drawn from them. An astrophysical jet operates over many decades in length scale, with different physics dominating at different distances from the source.

For reasons of computational feasibility, the 3D simulations that have been done so far use only a small range in distance, or a cylindrical geometry (e.g. Nakamura et al. 2001; Ouyed et al. 2003; Nakamura & Meier 2004). In the first case, the range of distance is too narrow to follow the consequences of 3-D instabilities effectively. In the second case, the effect of instability is limited by the boundaries. It is well known that kink instability can saturate into a finite amplitude, helical equilibrium when confined in a cylinder (in the astrophysical context see e.g. Königl and Choudhuri 1986; Lyubarskii 1999).

But a computational cylinder taylored to the size of the source covers a negligible range in length scales perpendicular to the axis, compared with an actual jet. If, instead, the simulations were done in a spherical or conical geometry, the continued expansion of the flow would stretch these helical configurations perpendicular to the axis, immediately making them unstable again. This is the rationale for our assumption that dissipation by instability will be a process that persists for a large distance along the jet.

It may be possible to make numerical progress in, say, a conical geometry, but limitations due to the finite range

in length scales and time scales that can be achieved will remain serious. For this reason, it is important to isolate physical effects that can not (yet) be included realistically in simulations, and explore them in more approximate models like the ones we have presented here.

6. Conclusions

The standard scenario for jet launching, acceleration and collimation involves large scale magnetic fields anchored to a rotating object (e.g. Blandford & Payne 1982; Sakurai 1985). The flow passes through three critical points, i.e. the slow, the Alfvén and the fast point. At the fast point the ratio of Poynting to matter energy flux is much larger than unity in the case of relativistic jets (Michel 1967; Camenzind 1986; Beskin et al. 1998) while further acceleration of the flow appears hard to achieve within ideal MHD except if the flow is decollimated (Li et al. 1992; Begelman & Li 1994).

In this work, we study how this picture is modified when one takes into account the fastest growing current driven instability, i.e. the $m = 1$ mode kink instability. We have modeled the instability by modifying the induction equation to account for non-ideal MHD processes and solving the relativistic MHD equations in the case of a radial flow. The instability is driven by B_ϕ, dissipates Poynting flux and has been shown to be an efficient mechanism to accelerate the flow.

The key parameter of the model is the ratio σ_0 of the Poynting to matter energy flux at the base of the flow. A large part of the AGN jet phenomenology can be understood in the context of this model for $\sigma_0 \sim$ several. On sub-pc scales the flow is Poynting-flux dominated with $B_\phi \gg B_r$. The flow is shown to be accelerated fast and to become matter dominated already at ∼pc scales, while it reaches terminal bulk factors of a few tens. The emission at the blazar zone can be a result of either internal shocks that take place in an unsteady flow, where fast shells catch up with slower ones, converting a small fraction of the bulk kinetic energy of the flow into radiation (Rees & Mészáros 1994; Spada et al. 2001), or direct manifestation of the energy released by the instability.

Within the same model, we propose that GRBs are a result of more Poynting flux dominated outflows with $\sigma_0 \sim$100. For these values of σ_0 the flow reaches terminal bulk Lorentz factors of the order of a few to several hundreds, while it remains moderately magnetized (i.e. $\sigma_\infty \sim 1$) at the afterglow region region. Although there is evidence for magnetized ejecta from afterglow modeling (e.g. Kumar & Panaitescu 2003; Zhang & Kobayashi 2005), more results are anticipated from early afterglow follow-ups that can test the model.

In the internal shock scenario for the prompt GRB emission, the shells collide at typical distances of $10^{13} - 10^{15}$ cm, where the flow is moderately Poynting-flux dominated. On the other hand, internal shock and Poynting-flux models exclude each other somewhat. If a strong magnetic field is added to an internally-shocked outflow, the radiative efficiency is further reduced with respect to that expected from the collision of unmagnetized shells (e.g. Fan et al. 2004). At the same time, dissipation in a predominantly magnetic outflow by instability (DC model) or internal reconnection (AC model) can produce radiation naturally at very high efficiency (up to 50%).

Acknowledgements. Giannios acknowledges support from the EU FP5 Research Training Network "Gamma Ray Bursts: An Enigma and a Tool."

References

Abramowicz, M. A., Novikov, I. D., & Paczyński, B. 1991, ApJ, 369, 175
Aloy, M. A., Janka, H.-T., & Müller, E. 2005, A&A, 436, 273
Appl, S., Lery, T., & Baty, H. 2000, A&A, 355, 818
Bateman, G. 1978, *MHD Instabilities*, Cambridge: MIT Press
Baty, H., & Keppens, R. 2002, ApJ, 580, 800
Begelman, M. C., & Sikora, M. 1987, ApJ, 322, 650
Begelman, M. C., & Li, Z.-Y. 1994, ApJ, 426, 269
Begelman, M. C. 1998, ApJ, 493, 291
Beskin, V. S., Kuznetova, I. V., & Rafikov, R. R. 1998, MNRAS, 299, 341
Bisnovatyi-Kogan, G. S., & Ruzmaikin, A. A. 1976, Ap&SS, 42, 401
Blandford, R. D. 1976, MNRAS, 176, 465
Blandford, R. D., & Znajek, R. L. 1977, MNRAS, 179, 433
Blandford, R. D., & Payne, D. G. 1982, MNRAS, 199, 883
Blinnikov, S. I., Novikov, I. D., Perevodchikova, T. V. & Polnarev, A. G. 1984, Sov. Astron. Lett., 10, 177
Bodo, D., Rosner, R., Ferrari, A., & Knobloch, E. 1989, ApJ, 341, 631
Bogovalov, S. V. 2001, A&A, 371, 1155
Burrows, D. N., Romano, P., Falcone, A., et al. 2005, Science, 309, 1833
Camenzind, M. 1986, A&A, 162, 32
Campana, S., Antonelli, L. A., Chincarini, G., et al. 2005, ApJ, 625, L23
Coroniti, F. V. 1990, ApJ, 349, 538
Daigne, F., & Drenkhahn, G. 2002, A&A, 381, 1066
Drenkhahn, G. 2002, A&A, 387, 714
Drenkhahn, G., & Spruit, H. C. 2002, A&A, 391, 1141
Eichler, D. 1993, ApJ, 419, 111
Eichler, D., Livio, M., Piran, T., & Schramm., D. N. 1989, Nature, 340, 126
Fan, Y. Z., Dai, Z. G., Huang, Y. F., & Lu, T. 2002, Chinese J. Astron. Astrophys., 2, 449
Fan, Y. Z., Wei, D. M., & Zhang, B. 2004, MNRAS, 354, 1031
Fendt, C., & Ouyed, R. 2004, ApJ, 608, 378
Ferrari, A., Trussoni, E., & Zaninetti, L. 1981, MNRAS, 196, 1051
Gabuzda, D. C., & Sitko, M. L. 1994, AJ, 107, 884
Giannios, D. & Spruit, H. C. 2005, A&A, 430, 1
Goldreich, P., & Julian, W. H. 1970, ApJ, 160, 971
Goodman, J. 1986, ApJ, 308, L47
Hardee, P. E., & Rosen, A. 1999, ApJ, 524, 650
Impey, C. D., Lawrence, C. R., & Tapia, S. 1991, ApJ, 375, 46
Janka, H.-T., Eberl, T., Ruffert, M., & Fryer, C. L. 1999, ApJ, 527, L39
Jaroszyński, M. 1993, Acta Astron., 43, 183
Kadomtsev, B. B. 1966, Rev. Plasma Phys., 2, 153

Kersalé, E., Longaretti, P.-Y., & Pelletier, G. 2000, A&A, 363, 1166
Kluźniak, W., & Ruderman, M. 1998, ApJ, 505, L113
Königl, A., & Choundury, A. R. 1985, ApJ, 289, 173
Königl, A., & Granot, J. 2002, ApJ, 574, 134
Kumar, P. 1999, ApJ, 523, 113
Kumar, P., & Panaitescu, A. 2003, MNRAS, 346, 905
Lery, T, Baty, H., & Appl S. 2000, A&A, 355, 1201
Li, L.-X. 2002, ApJ, 564, 108
Li, Z.-Y., Begelman, M. C., & Chiuch, T. 1992, ApJ, 384, 567
Lloyd-Ronning, N. M., & Zhang, B. 2004, ApJ, 613, 477
Longaretti, P.-Y. 2003, Phys. Lett. A, 320, 215
Lovelace, R. V. E. 1976, Nature, 262, 649
Lyubarskii, Yu. E. 1999, MNRAS, 308, 1006
Lyubarsky, Y., & Kirk, J. G. 2001, ApJ, 547, 437
Lyutikov, M. 2001, Phys. Fluids, 14, 963
Lyutikov, M., & Blandford R. D. 2003, astro-ph/0312347
Lyutikov, M. 2005, astro-ph/0512342
MacFadyen, A., & Woosley, S. E. 1999, ApJ, 524, 262
Mestel, L. 1968, MNRAS, 138, 359
Michel, F. C. 1969, ApJ, 158, 727
Mochkovitch, R., Hernanz, M., Isern, J., & Martin, X. 1993, Nature, 361, 236
Moderski, R., Sikora, M., & Błażejowski, M. 2003, A&A, 406, 855
Nakamura, M., Uchida, Y., & Hirose, S. 2001, New Astron., 6, 61
Nakamura, M., & Meier, D. L. 2004, ApJ, 617, 123
Nartallo, R., Gear, W. K., Murray, A. G., et al. 1998, MNRAS, 297, 667
Nousek, J. A., Kouveliotou, C., Grupe, D., et al. 2005, ApJ, submittied (astro-ph/0508332)
Ouyed, R., Clarke, D. A., & Pudritz, R. E. 2003, ApJ, 582, 292
Paczyński, B. 1986, ApJ, 308, L43
Panaitescu, A., Spada, M., & Mészáros, P. 1999, ApJ, 522, 105
Panaitescu, A., & Kumar, P., 2002, ApJ, 571, 779
Panaitescu, A., Mészáros, P., Gehrels, N., Burrows. D., & Nousek, J. 2005, MNRAS, in press (astro-ph/0508340)
Pe'er, A., Rees, M. J., & Mészáros, P. 2005, ApJ, 635, 476
Piran, T. 1999, Phys. Rep., 314, 575
Ray, T. P. 1981, MNRAS, 196, 195
Rees, M. J., & Mészáros, P. 1994, ApJ, 430, L93
Rees, M. J., & Mészáros, P. 2005, ApJ, 628, 847
Rhoads, J. E. 1997, 487, L1
Ryde, F. 2005, ApJ, 625, L95
Sakurai, T. 1985, A&A, 152, 121
Sakurai, T. 1987, PASJ, 39, 821
Sari, R., Piran, T., & Halpern, J. P. 1999, ApJ, 519, L17
Sikora, M., Begelman, M. C., & Rees, M. J. 1994, ApJ, 421, 153
Sikora, M., Begelman, M. C., Madejski, M. G., & Lasota, J-P. 2005, ApJ, 625, 72
Spada, M., Ghiselini, G., Lazzati, D., & Celloti, A. 2001, MNRAS, 325, 1559
Spruit, H. C. 1999, A&A, 341, L1
Spruit, H. C., Foglizzo, T., & Stehle, R. 1997, MNRAS, 288, 333
Spruit, H. C., Daigne, F., & Drenkhahn, G. 2001, A&A, 369, 694
Spruit, H. C., & Drenkhahn, G. 2003, Magnetically powered prompt radiation and flow acceleration in GRB, in Proceedings "Gamma Ray Bursts in the Afterglow Era, Third Workshop" (Rome, Sept. 2002) p. 357 (astro-ph/0302468)
Tagliaferri, G., Goad, M., Chincarini, G., et al. 2005, Nature, 436, 985
Thompson, C. 1994, MNRAS, 270, 480
Usov, V. V. 1992, Nature, 357, 472
Vlahakis, N., & Königl 2003a, ApJ, 596, 1080
Vlahakis, N., & Königl 2003b, ApJ, 596, 1104
Weber, E. J., & Davis, L. 1967, ApJ., 148, 217
Woosley, S. E. 1993, ApJ, 405, 273
Zhang, B., Kobayashi, S., & Mészáros, P. 2003, ApJ, 595, 950
Zhang, B., & Kobayashi, S. 2005, ApJ, 628, 315
Zhang, B., Fan, Y. Z., Dyks, J., et al., 2005, ApJ, in press (astro-ph/0508321)